PERGAMON

Vision Research 39 (1999) 2213–2227

Vision Research

The perception and discrimination of speed in complex motion

Colin W.G. Clifford [1], Scott A. Beardsley, Lucia M. Vaina *

Brain & Vision Research Laboratory, Department of Biomedical Engineering, Boston University, Boston, MA 02215, USA

Received 8 June 1998; received in revised form 12 November 1998

Abstract

Random dot kinematograms were used to simulate radial, rotational and spiral optic flow. The stimuli were designed so that, while dot speed increased linearly with distance from the centre of the display, the density of dots remained uniform throughout their presentation. In two experiments, subjects were required to perform a temporal 2AFC speed discrimination task. Experiment 1 measured the perceived speed of a range of optic flow patterns against a rotational comparison stimulus. Radial motions were found to appear faster than rotations by approximately 10%, with a smaller but significant effect for spirals. Experiment 2 measured discrimination thresholds for pairs of similar optic flow stimuli identical in all respects except mean speed. No consistent differences were observed between the speed discrimination thresholds of radial, rotational and spiral motions and a control stimulus with the same speed profile in which motion followed fixed random trajectories. The perceived speed results are interpreted in terms of a model satisfying constraints on motion-in-depth and object rigidity, while speed discrimination appears to be based upon the pooled responses of elementary motion detectors.

Keywords: Complex motion; Speed perception; Optic flow; Visual cortex; Psychophysics; Random dots

1. Introduction

Several recent papers have reported illusions in perceived speed involving complex motion stimuli. Geesaman and Qian (1996, 1998) found that expanding random dot patterns appear to move faster than corresponding rotations and translations by approximately 30%, while Bex and colleagues found that the speed of radial gratings relative to translational gratings is overestimated by 20–60% (Bex and Makous, 1997; Bex, Metha & Makous, 1998). Interestingly, the two groups proposed different interpretations of their results:

(1) Geesaman and Qian (1996) suggested that the illusory difference in perceived speed of expansions and rotations might be a perceptual correlate of a reported anisotropy in the response selectivity of neurons in the dorsal region of the primate medial superior temporal area (MSTd). MSTd neurons have consistently been found to respond preferentially to particular patterns of large-field motion such as expansions, contractions, rotations and spirals (Saito, Yukie, Tanaka, Hikosaka, Fukada & Iwai, 1986; Tanaka, Hikosaka, Saito, Yukie, Fukada & Iwai, 1986; Tanaka, Fukada & Saito, 1989; Tanaka & Saito, 1989; Duffy & Wurtz, 1991a,b; Orban, Lagae, Verri, Raiguel, Xiao, Maes & Torre, 1992; Graziano, Anderson & Snowden, 1994; Geesaman & Andersen, 1996). MSTd cells exhibit a continuum of preferred responses to complex motion stimuli, but the distribution of response selectivities is biased in favour of expansion (Graziano et al., 1994; Geesaman & Andersen, 1996). Thus, a relationship between the strength of the neural response in MSTd and speed perception in optic flow stimuli might account for the illusory difference in perceived speed between expansion and rotation. We term this the **neural response bias** hypothesis.

(2) Bex and Makous (1997) observed that radial motion stimuli do not appear to lie flat in the plane of the display, but rather are seen to move in depth relative to the observer. Expanding stimuli are typically perceived as expanding while at the same time approaching the observer, and contracting stimuli are seen as simultaneously contracting and receding in depth. The speed of the perceived motion of the stimulus

* Corresponding author. Tel.: +1-617-353-2455; fax: +1-617-353-6766; e-mail: vaina@bu.edu.

[1] Present address: Psychology Department, School of Behavioural Sciences, Macquarie University, Sydney, NSW 2109, Australia.

0042-6989/99/$ - see front matter
PII: S0042-6989(98)00314-9

through three-dimensional space would then depend on the degree of perceived motion-in-depth as well as the actual speed of the stimulus in the plane of the display. If observers base their judgments of stimulus speed on the visual interpretation of motion in a 3-D environment, rather than its 2-D retinal projection, then the difference in perceived speed between radial and translational or rotational motion might reflect the fact that motion-in-depth is perceived with radial motions but not with rotations and translations. We term this the **motion-in-depth** hypothesis.

The results of Geesaman and Qian (1996, 1998), Bex and Makous (1997) and Bex et al. (1998) demonstrate that perceived speed depends upon the global pattern of motion. Maps of complex motion selectivity have been reported in the superior temporal sulcus, with cortical columns of neurons preferring similar complex motions (Geesaman, Born, Anderson & Tootell, 1997). Analysis of the distribution of preferred responses in MSTd also indicates a clustering of cells with similar selectivities (Lagae, Maes, Raiguel, Xiao & Orban, 1994), with a strong bias toward expanding motions suggesting a role in visually-guided navigation (Graziano et al., 1994). It has recently been reported that a large majority of MSTd neurons prefer stimuli containing a speed gradient to those in which all dots move at the same speed, strengthening the view that MSTd is involved in the analysis of optical flow (Duffy & Wurtz, 1997). In other species, cells selective for complex patterns of motion have been reported in the lobula plate of the blowfly (Krapp & Hengstenberg, 1996), the accessory optic system and vestibulocerebellum of the pigeon (Wylie, Bischof & Frost, 1998) and the lateral suprasylvian visual area of the cat (Kim, Mulligan & Sherk, 1997; Mulligan, Kim & Sherk, 1997).

Previous psychophysical studies have found evidence for the existence of specialized detectors sensitive to radial, rotational, and translational motion (Regan & Beverley, 1985; Freeman & Harris, 1992; Morrone, Burr & Vaina, 1995; Snowden & Milne, 1996, 1997). The results of these and other experiments suggest that these specialized detectors integrate local motions to obtain a global motion percept (Watamaniuk & Sekuler, 1992; Smith, Snowden & Milne, 1994; Morrone et al., 1995). However, studies of speed discrimination thresholds in random kinematograms (Sekuler, 1992) and sinusoidal grating stimuli (Bex et al., 1998) have shown that thresholds for expanding, rotational and linear motion are all similar. Sekuler (1992) found that summation among motion elements in expanding displays never exceeds predictions based upon simple pooling rules. On this basis, Sekuler (1992) argued that speed discrimination might be based on the pooling of unidirectional local motion signals without the need to postulate the existence of specialised complex motion detectors. Although subsequent psychophysical evidence strongly suggests the existence of global motion detectors (Morrone et al., 1995; Snowden & Milne, 1996, 1997), it is possible that such detectors do not contribute to speed discrimination performance.

Here, we measure perceived speed and speed discrimination thresholds for a range of optic flows (expansions, expanding spirals, rotations, contracting spirals, and contractions), and speed discrimination thresholds for a set of speed-matched control stimuli from which the speed gradient and/or the directional information has been removed. The perceived speed experiment can be seen as an extension of those carried out by Geesaman and Qian (1996, 1998) to encompass a wider range of optic flow stimuli, while the speed discrimination experiment expands upon the work of Sekuler (1992). While Bex et al. (1998) investigated perceived speeds and speed discrimination thresholds for radial and rotational grating stimuli, ours is the first study using stimuli containing radial speed gradients to measure both perceived speed and speed discrimination thresholds across a range of optic flows. The stimuli we use are random dot kinematograms carefully constructed to sample continuous time optic flow motions at discrete time intervals. Optic flow stimuli of different types are matched for speed such that all stimuli of the same speed contain identical radial speed gradients and polar direction gradients. A novel wraparound procedure for dots leaving the stimulus aperture ensures that dot density remains constant over area for the entire stimulus duration, thus avoiding contamination with spatial cues. Our results are compared with predictions based on: (a) the **neural response bias** hypothesis—distributed coding over a population of units selective to particular optic flows, but with an over-representation of expansion-selective units; (b) an elaboration of the **motion-in-depth** hypothesis—a model implementing simultaneous constraints on motion-in-depth and object rigidity.

2. General methods

2.1. Stimuli

Random dot kinematogram (RDK) stimuli were generated on a Power Macintosh 8500/120 and presented on an AppleVision 1710 monitor in a 24° diameter annular region (central 4° removed) at a 54 cm viewing distance. RDK movie sequences were generated off-line and presented with a screen resolution and refresh rate of 832×624 pixels and 75 Hz, respectively.

Under default conditions, each RDK contained a uniform distribution of 190 (9.3 cd deg^{-1} m^{-2}) motion dots displayed on a low luminance (5.2 cd deg^{-1} m^{-2}) gray background. At the viewing distance each dot subtended 10 min of visual angle and moved through a

radial speed gradient whose mean speed could be varied between tests in a direction consistent with the type of complex motion being displayed.

The motion of the dots in the RDK was determined as though the trajectory of each dot had been first calculated in the continuous-time domain (see Appendix A). The position of each dot in each frame of the RDK was then obtained by sampling from the continuous time trajectory at discrete time intervals corresponding to the refresh time of the display. This was necessary because, in order to maintain a constant global velocity field in an optic flow stimulus, the motion of each local feature in the stimulus must accelerate. For example, in a pattern expanding at a constant velocity, each feature accelerates centrifugally such that its speed is proportional to its distance from the focus of expansion. In a pattern rotating at a constant angular velocity, the speed of each feature remains constant over time but its direction of motion changes such that it accelerates centripetally. To represent the motion of an accelerating dot between a pair of discrete frames, it is not sufficient simply to calculate the velocity of the dot corresponding to its position in the first frame and to multiply this by the time between frames. To do so implicitly assumes that the velocity of the dot between frames is constant, not accelerating. Thus, we calculated dot positions by sampling from continuous-time trajectories in which the dots were accelerating at all times. In this way we were able to match the speeds of different types of complex motion stimuli precisely.

The experimental tasks controlled for timing-based discrimination by including stimulus duration uncertainties which were proportional to and centered around the nominal stimulus duration. Uncertainties in the stimulus duration spanned a frame count which was 1/6 of the nominal stimulus duration (33 ± 3 frames; 440 ± 40 ms).

To promote a global discrimination task, motion discrimination based on the trajectories of single dots was reduced by assigning dot lifetimes of 11 frames (156 ms). Coherent stimulus flicker was minimized by uniformly distributing the initial dot ages between 1 and 11 frames. When dots exceeded the lifetime or moved beyond the aperture boundaries they were assigned new positions and trajectories consistent with the optic flow type and the maintenance of a constant dot density over the stimulus.

Details of the trajectory calculations and constant density wraparound procedure are given in Appendix A.

2.2. Procedure

In both experiments, subjects performed a temporal two-alternative, forced-choice speed discrimination task on a constant set of optic flow stimuli. The experiments were conducted in a darkened room. Prior to the start of each test, subjects adapted for 10 s to the background display in the low luminance environment. After adaptation, pairs of stimuli were presented for 440 ± 40 ms with a 500 ms interstimulus interval while subjects fixated on a small square placed at the center of the stimulus aperture. An auditory cue preceded each stimulus. Subsequent to the presentation of each stimulus pair, subjects were required to discriminate the speed of the two stimuli by pressing a button which corresponded to the faster stimulus.

During testing, optical flow stimuli of different types were interleaved to minimize the build-up of adaptation to specific complex motions (expansion, contraction, rotation, etc.). Within each experimental trial, each stimulus pair from the interleaved set was presented a fixed number of times (eight for Experiment 1; 16 for Experiment 2). For each test condition, percent correct values were calculated for the stimulus pairs in each trial and used to plot psychometric functions for each optic flow type.

2.3. Observers

A total of three subjects participated in the experimental tasks. All had normal or corrected-to-normal vision. Two authors of this study, CC and SB, were experienced psychophysical observers. A first-time psychophysical observer naïve to the purposes of the study, CL, was tested on the perceived speed task.

3. Experiment 1

3.1. Perceived speed of complex motion

The purpose of Experiment 1 was to measure the perceived speeds of a range of optic flow stimuli. Subjects performed a temporal 2AFC speed discrimination. Rotational motion at a mean speed of 21.3 deg s^{-1} was chosen as the comparison stimulus. The comparison stimulus was always presented before the test stimulus in each pair, but the direction of rotation of the comparison stimulus was randomised from stimulus pair to stimulus pair. The test stimuli used were expansions, contractions, expanding spirals, contracting spirals, and rotations. The speed of the test stimulus was varied between $\pm 35\%$ of the speed of the comparison stimulus. A logistic function was fitted to the data from each trial for each type of complex motion using a non-linear least squares procedure, and the 50% point of the fitted function was taken as a measure of the perceived speed of the test stimulus relative to the rotational comparison stimulus. This procedure was repeated at least six times for each complex motion, and the mean 50% point and its associated standard error calculated.

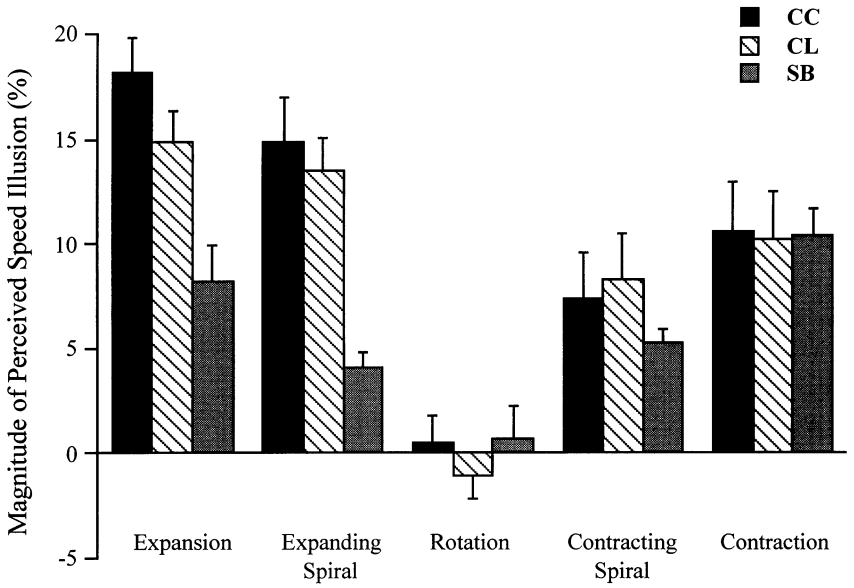

Fig. 1. The magnitude of the perceived speed illusion for three subjects over a range of optic flow stimuli. The mean dot speed in the rotating comparator stimulus was 21.3 deg s^{-1}. The magnitude of the illusion was computed as the average across runs of the amount by which the speed of the rotational comparator exceeded the speed of the test stimulus at the point of subjective equality, expressed as a percentage of the actual speed of the test. Error bars here and in subsequent figures are ± 1 SE.

Data presented in terms of the magnitude of the perceived speed illusion are shown in Fig. 1. The magnitude of the perceived speed illusion is calculated as the amount by which the speed of the rotational comparison stimulus exceeds the speed of the test stimulus at the point of subjective equality. For all subjects the magnitude of the perceived speed illusion for all radial and spiral motions was significantly greater than zero ($P < 0.001$), while for the rotational test stimuli the magnitude was always within one standard error of zero. A two-way analysis of variance was used to examine whether there were significant differences in perceived speed between: (1) expanding motions (expansions and expanding spirals) and contracting motions (contractions and contracting spirals); (2) radial motions and spirals. The ANOVA reveals that expanding motions were perceived as significantly faster than contracting motions by subjects CC and CL, but not by SB (CC: $F_1 = 13.47$, $P < 0.01$; CL: $F_1 = 6.60$, $P < 0.05$; SB: $F_1 = 0.31$, $P > 0.1$). While all subjects tended to perceive radial motions faster than the corresponding spirals, the difference is only statistically significant for SB (SB: $F_1 = 11.62$, $P < 0.01$; CC: $F_1 = 2.50$, $P > 0.1$; CL: $F_1 = 0.78$, $P > 0.1$). None of the subjects' data showed significant interactions between the two factors (expanding/contracting and radial/spiral).

Fig. 2 shows perceived speed data for a baseline mean speed of 6.4 deg s^{-1} alongside the 21.3 deg s^{-1} data for two subjects, CC and SB (it should be noted that the scales on the ordinates of the two plots are different). The data for both subjects shows a similar trend across the two base speeds. For expanding stimuli, there are no significant differences between the data at the two speeds. For contracting stimuli, the magnitude of the perceived speed illusion for both CC and SB decreases between the 21.3 and 6.4 deg s^{-1} conditions and is not significantly different from zero for the slower contracting spirals. In all cases, as would be expected, the rotation data does not differ significantly from zero.

4. Experiment 2

4.1. Speed discrimination in complex motion

Speed discrimination thresholds were measured for a range of optic flow stimuli and a set of matched controls. Subjects were required to perform a temporal 2AFC speed discrimination task between stimuli undergoing similar motions. The comparison stimuli had a mean speed of 21.3 deg s^{-1}. Pairs of stimuli with different motions were interleaved in a random sequence, and the order of presentation of the test and comparison stimuli was randomised from stimulus pair to stimulus pair. For each type of complex motion in each trial, a logistic function of the difference in test and comparator speeds was fitted to the percentage correct data and its 75% point taken as a measure of the discrimination threshold. This procedure was repeated several times for each complex motion, and the mean threshold and its associated standard error calculated.

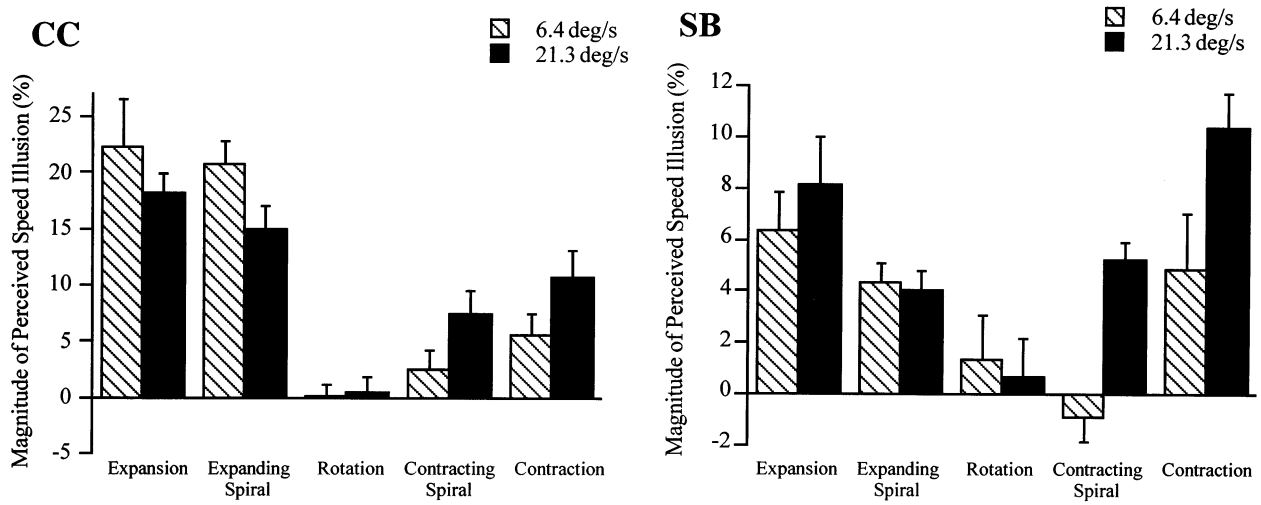

Fig. 2. The magnitude of the perceived speed illusion for subjects CC and SB at two different base speeds: 6.4 and 21.3 deg s^{-1}. Note the different scales on the ordinates of the two plots.

Speed discrimination data for two subjects, CC and SB, are presented in Fig. 3 as a percentage of the speed of the comparison stimulus for five optic flows. For both subjects, speed discrimination thresholds were approximately 4% of the baseline speed with no consistent trend as a function of stimulus type. Across stimulus types, the mean speed discrimination threshold was 3.66% for CC and 4.48% for SB, with no significant outliers.

Speed discrimination thresholds were also measured on a set of speed-matched control stimuli. In the 'random speed' controls, the speeds of the dots were randomised so that the overall distribution of speeds was the same as for the optic flow stimuli but the radial gradient in dot speed was no longer present. The direction of motion of the dots was left unchanged, and random speed expansions and contractions were generated. In the 'random direction' controls, the direction of motion of each dot was randomly assigned uniformly over the range of 0–360° but dot speed remained consistent with the speed profile in the optic flow stimuli, increasing linearly with distance from the centre. Two random direction control stimuli were generated: Random walk (RW) and fixed random trajectory (FRT). In the RW stimulus the direction of motion of each dot was randomly reassigned at each frame, while dots in the FRT stimulus moved in a single randomly selected direction for the duration of their lifetime. A random speed version of the FRT stimulus was also presented in which there was neither a speed gradient nor a pattern of directional information.

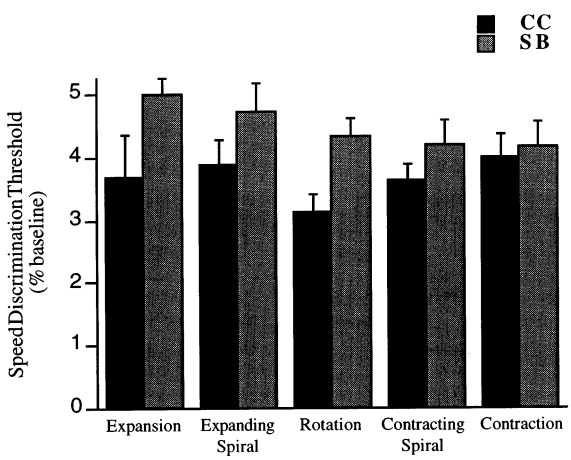

Fig. 3. Speed discrimination thresholds, expressed as percentage of the speed of the comparator, for subjects CC and SB over a range of optic flow stimuli. The mean dot speed in the compator stimuli was 21.3 deg s^{-1}.

Fig. 4 compares subjects' speed discrimination thresholds for radial motions with performance over a set of control stimuli. The data from both subjects shows the same trends. Speed discrimination thresholds for fixed random trajectory motion with a speed gradient are not significantly different from those for the optic flow stimuli ($\sim 4\%$). Thresholds for the random speed stimuli are consistently higher than for the corresponding motions containing a radial speed gradient. Thresholds for the random walk stimuli are significantly higher (6–8%) than for the other speed gradient stimuli.

5. Discussion

The data from Experiment 1 show a variation in perceived speed as a function of the type of optic flow stimulus: radial and spiral motions are consistently seen as moving faster than corresponding rotations, radial motions tend to appear faster than spirals, and expand-

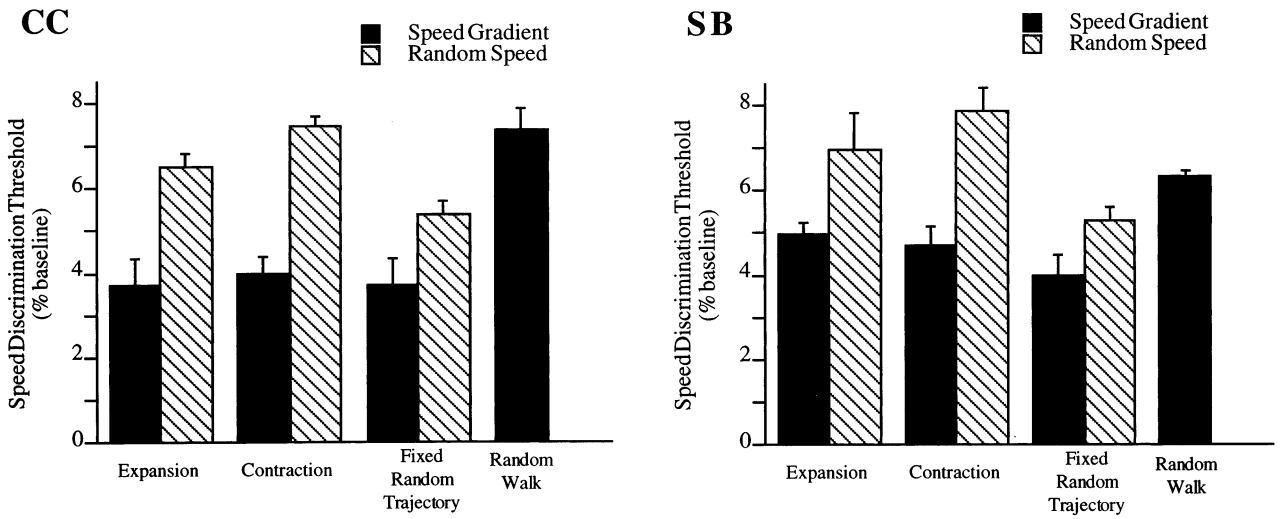

Fig. 4. Speed discrimination thresholds for subjects CC and SB on a set of control stimuli. For expansions and contractions, speed discrimination thresholds for 'random speed' stimuli are shown alongside thresholds for corresponding optic flow stimuli containing a radial speed gradient. In the random speed stimuli, the direction information and overall speed profile of the optic flow stimuli is conserved, but the speed gradient is removed by re-randomising the distance of each dot from the centre of the stimulus after its speed has been assigned. The two 'random direction' stimuli contain the same speed gradient as the optic flow stimuli, but dot direction is randomised. For the 'fixed random trajectory' stimulus, each dot moves in a single direction throughout its lifetime, while for the 'random walk' stimulus dot direction is randomly reassigned afresh at frame.

ing stimuli tend to be perceived as faster than corresponding contracting stimuli. Experiment 2 shows that there is no systematic effect of complex motion pattern on speed discrimination, and that removing directional information does not affect speed discrimination thresholds.

What mechanisms underlie the illusory variation in perceived speed as a function of optic flow type? One possibility, put forward by Geesaman and Qian (1996), is that it reflects the number of complex motion detectors tuned to particular types of optic flow stimuli (the **neural response bias** hypothesis). Another hypothesis is that the perceived speed of complex motion patterns is related to the perception of **motion-in-depth** (Bex & Makous, 1997; Bex et al., 1998). We discuss these two theories below.

Graziano et al. (1994) found that the preferred tunings of cells in rhesus monkey MSTd are strongly biased towards expansions. Fig. 5 shows the preferred directions of the 57 cells found by Graziano et al. (1994) to show a single peak in preferred tuning (redrawn from Zemel and Sejnowski (1998)). If the human visual system is also biased towards expansion in the tuning of its complex motion detectors, then a simple relationship between the activity of MSTd and the perceived speed of complex motions predicts that expansions would be perceived as faster than other optic flows, while rotations and contractions would appear to move at similar rates.

The results of our Experiment 1 confirm the finding of Geesaman and Qian (1996) and Bex et al. (1998) that expansion appears faster than rotation. However, Experiment 1 also shows that contraction is perceived as significantly faster than rotations. Graziano et al. (1994) found similar numbers of MSTd cells preferentially sensitive to each direction of rotation as were tuned to contraction, so a simple relationship between complex motion detector activity and speed perception would predict little or no difference in perceived speed between contractions and rotations. In order to defend the **neural response bias** hypothesis, one would have to argue that the number of cells studied by Graziano et al. (1994) do not constitute a sufficiently large sample to rule out the possibility of a smaller population bias to contractions (in addition to the expansion bias), or that such a bias might be present in humans even if not

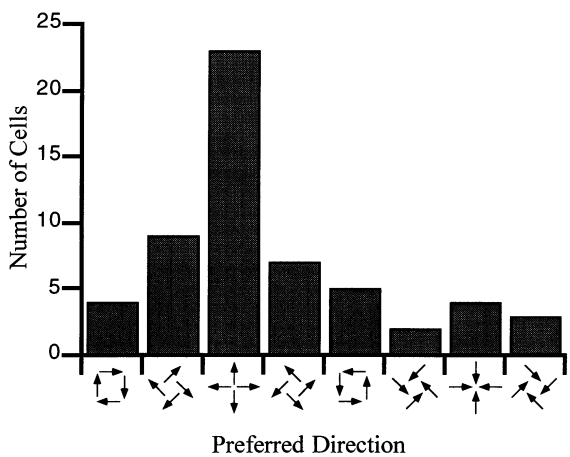

Fig. 5. Histogram of the preferred optic flow stimuli for 57 MSTd cells in the Graziano et al. (1994) study (redrawn from Zemel & Sejnowski, 1998).

in all primates. A secondary bias towards contractions in the tuning of MSTd neurons has been reported by Geesaman and Andersen (1996), making it impossible to reject the **neural response bias** hypothesis on this basis, although it should be noted that in the Geesaman and Andersen (1996) study the number of cells preferring contractions is still only half the number preferring expansions.

It is interesting to note that the magnitude of the perceived speed effect we observed between expansions and rotations was consistently smaller than the 32% reported by Bex et al. (1998). A possible reason for the difference in magnitude of the perceived speed illusion between that reported here and the Bex et al. (1998) study might be that in our Experiment 1 the rotational comparison stimulus was always presented first, rather than in a random order. However, a dependence of perceived speed judgments on stimulus order has recently been reported (Geesaman & Qian, 1998) such that the magnitude of the effect is greater when the expansion is presented **after** the rotation, as here. Thus it would appear that some other element of the experimental procedure must underlie the difference in reported magnitudes of the perceived speed illusion.

Does the **neural response bias** hypothesis make any predictions regarding our ability to discriminate the speed of complex motions? If the activity of a population of complex motion detectors in our visual system determines the perceived speed of optic flow stimuli, then this suggests that our ability to discriminate the speeds of two such stimuli will depend on the difference in the response they generate. We might, then, expect to be better at discriminating motions which strongly activate our complex motion detectors. The results of Experiment 2 show that this is not the case: speed discrimination thresholds show no systematic variation with type of optic flow stimulus.

The speed discrimination thresholds for optic flow measured in Experiment 2 are in the range of 3–5%, similar to those reported for translational stimuli (McKee, 1981; De Bruyn & Orban, 1988). Studies by Sekuler (1992) and Bex et al. (1998) have shown that speed discrimination thresholds are similar for radial, rotational and translational motion. However, there is psychophysical and physiological evidence for global motion detectors tuned to translational motion (Duffy & Wurtz, 1991a,b; Morrone et al., 1995). Speed discrimination in translational stimuli is thus not necessarily due only to local motion processing. To investigate whether speed discrimination in complex motion patterns is mediated by pooling the outputs of local motion detectors, as proposed by Sekuler (1992), or whether complex motion detectors are involved, we designed control stimuli in which the speed of motion was locally identical to that of the complex motion stimuli but in which direction was randomised. In the fixed random trajectory (FRT) stimulus, dots moved in a single (randomly assigned) direction throughout their lifetimes, while in the random walk (RW) stimulus, dot direction was reassigned randomly on a frame-by-frame basis.

Speed discrimination thresholds for the FRT are no higher than for the optic flow stimuli (see Fig. 4). Since the fixed random trajectory controls are matched for speed with the optic flow stimuli, but contain no pattern of directional information, this suggests that information on the global pattern of direction motion provided by complex motion detectors is not used in tasks of speed discrimination. The speed discrimination thresholds for the RW stimuli are higher than for FRT and the optical flow stimuli, presumably because the rapid changes in direction of the dots in the RW stimuli (every 13 ms) allow only very limited temporal integration. In the random speed controls, the overall speed distribution of the dots is the same as in the optic flow stimuli but their positions are random over space rather than in accord with a global speed gradient. The higher speed discrimination thresholds for random speed stimuli show that the presence of a speed gradient within the stimulus facilitates speed discrimination.

How might the presence of a speed gradient facilitate speed discrimination? One difference between the speed gradient and random speed stimuli is that, in the presence of a speed gradient, the speed of a dot at any given location is precisely defined. This in turn means that the speed of a dot at any given location defines the speed of the stimulus as a whole. In the presence of a speed gradient, the speed discrimination task could in principle be carried out by comparing the speed of motion in a small region of the stimulus. In the random speed stimuli, dot speeds are ascribed randomly without regard to dot position, so the relative speeds of dots at corresponding locations in a stimulus pair are only loosely related to the relative speeds of the two stimuli as a whole. Since speed is no longer correlated with radial position, comparisons based on a small region are not sufficient for accurate speed discrimination. In order to extract the most accurate possible speed estimate from a random speed stimulus it would be necessary to pool information across the entire stimulus. However, unpublished data from this laboratory show that, even in the presence of a speed gradient, performance on the speed discrimination task improves with increasing stimulus area up to at least half of that used here. This suggests that speed discrimination for stimuli containing a speed gradient is not limited to comparisons within a small region. Thus the increased speed discrimination thresholds in the absence of a speed gradient cannot be attributed to a limit on the extent of spatial pooling of local motion signals.

An alternative explanation of the fact that speed discrimination thresholds are lower in the presence of a

speed gradient is that local motion signals might be pooled in such a way that stimuli containing speed gradients produce a more homogeneous distribution of signals at the pooling stage. It is known that the receptive field sizes of direction-selective cells in primate visual cortex increase as a function of eccentricity (Albright & Desimone, 1987), and psychophysical studies have shown that aspects of human motion perception scale in a corresponding manner (van der Grind, van Doorn & Koenderink, 1983). Harris, Freeman and Tyler (1994) found that estimates of the temporal proximity of random dot patterns were more accurate in the presence of radial speed gradients than when they were removed. If the spatial but not the temporal properties of motion detectors scale with eccentricity, then detectors at different retinal eccentricities will respond with similar intensity when presented with stimuli containing a speed gradient. Such an architecture would be well-suited to calculating the temporal proximity or time-to-contact of looming objects without first computing speed explicitly (Lee, 1980), and would be consistent with the results of Harris et al. (1994). In the context of Experiment 2, stimuli containing a radial speed gradient would excite motion detectors at different eccentricities to the same degree, while the response to random speed stimuli would vary with eccentricity. The distribution of signal strengths in the random speed case would then be much broader, making discrimination of stimuli with similar speeds correspondingly harder.

We propose that the discrimination of speed in optic flow stimuli is neither mediated by complex motion detectors per se, nor based on local estimates of speed, but depends instead upon the pooled responses of elementary motion detectors. To draw this conclusion is not, of course, to deny the existence of complex motion detectors, but simply to suggest that they do not mediate speed discrimination. Motion-sensitive mechanisms are known to exist at many levels of the visual system (see Snowden (1994) for a review), and Experiment 2 suggests that speed discriminations can be made accurately on the basis of responses early in the motion processing hierarchy. Is it possible that different areas of the brain mediate the perception and discrimination of speed? If we are to reconcile the **neural response bias** hypothesis for perceived speed with the results of Experiment 2, then this would suggest that the mechanisms which mediate speed discrimination are distinct from, and prior in the motion hierarchy to, complex motion detectors in the human visual system.

Alternatively, perhaps differences in perceived speed across optic flows are related to our perception of **motion-in-depth** in certain complex motion patterns (Bex & Makous, 1997; Bex et al., 1998). Global motion patterns such as expansions are projected onto our retinas as we move through the world. Commonly, an expanding optic flow field will correspond not to an object physically deforming in front of our eyes, but to a rigid object approaching us or which we are approaching. If observers base their judgments of perceived speed on the visual interpretation of motion in a 3-D environment, rather than on its 2-D retinal projection, then different interpretations of optic flows in terms of motion-in-depth will give rise to differences in perceived speed.

How do our visual systems distinguish between rigid objects moving in depth and objects deforming physically? It has been shown by Verghese and Stone (1995, 1996) that speed discrimination appears to depend upon the parsing of the stimulus in terms of objects. Perhaps the perception of depth-from-motion is due to the parsing of retinotopic motion information by higher-level mechanisms tuned to patterns of global motion (De Bruyn & Orban, 1990). If the optic flow has a radial component, then this could be due either to motion-in-depth or to deformations of objects in the visual scene. In the experiments conducted here, the visual environment is relatively impoverished (white dots moving on a grey screen in a darkened room) and offers only minimal cues as to the most appropriate interpretation of the pattern of optic flow at the retina due to the dots' motion: is there a fixed pattern of dots moving relative to us in depth, or is there an expanding pattern of dots at a fixed distance from us? These are the two extremes in a continuum of possible interpretations consistent with the retinal positions and motions of the dots (Fig. 6). When we view a radial motion stimulus, we certainly perceive it as moving in depth, but at the same time we also perceive the dot pattern expanding or contracting in the plane of the stimulus. We suggest that, in such cases, the pattern of motion is interpreted such that it satisfies as closely as possible two interdependent constraints: (a) a minimum motion-in-depth constraint; (b) a minimum object deformation constraint. Constraint (a) can be thought of as an a priori disposition to see a uniform grey field as static rather than moving in depth, and constraint (b) as a tendency to see objects in the world moving rigidly rather than deforming.

The joint minimisation of the departure from a minimum motion-in-depth constraint and a constraint on deformation (non-rigidity) within the plane of the stimulus can be set up as the minimisation of a cost function, H, given by:

$$H = \lambda\left(\frac{\Delta z}{z}\right)^2 + (1-\lambda)(\alpha_p - 1)^2 \quad (1)$$

where z is the distance of the screen from the observer and Δz is the perceived change in depth in a time Δt. The value of α_p corresponds to the perceived scaling of the stimulus between frames ($\alpha_p > 1$ for expansion within the plane of the stimulus; $\alpha_p < 1$ for contraction; $\alpha_p = 1$ for rigidity, i.e. no deformation within the

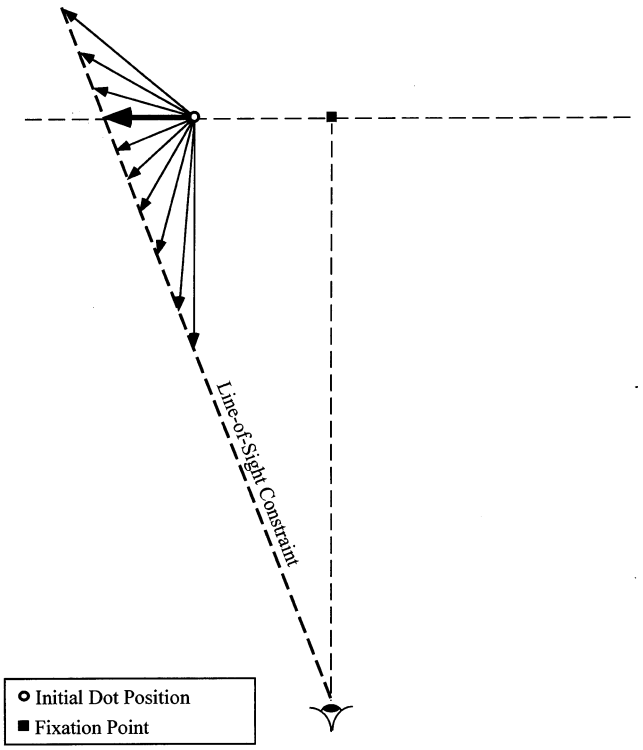

Fig. 6. Schematic diagram of the possible interpretations of motion in the random dot kinematograms. The observer fixates a stationary point at the centre of the display screen. The figure illustrates the case for a single dot moving centrifugally in the plane of the screen. The actual motion of the dot is represented by the bold arrow. The perceived motion of the dot is constrained by the position of its projection onto the retina to lie on a line in 3-D space, which we term the line-of-sight constraint. The arrows represent possible perceived trajectories of the dot in 3-D space. For example: the dot may be perceived to be moving in the plane of the display, corresponding to its actual motion; the dot could in principle be perceived as moving perpendicularly out of the screen towards the observer; the perceived motion of the dot may involve components both within and perpendicular to the screen. We propose that perceived stimulus speed corresponds to the length of the perceived dot trajectory in 3-D space, with longer arrows in the diagram representing faster speeds. Which trajectory and speed are actually perceived depends upon the way in which the retinal image is interpreted based upon implicit constraints in our visual systems.

plane). The parameter λ determines the relative weighting attached to the two constraints. If $\lambda = 1$, motion-in-depth is penalised strongly while deformation within the plane has a zero weighting, so the motion of the dot patterns will always be seen within the plane of the stimulus with no depth component. If $\lambda = 0$, motion-in-depth will have zero cost and so the dot patterns will always be seen as moving rigidly ($\alpha_p = 1$) even if that corresponds to a very rapid motion-in-depth.

We investigated what this simple constraint satisfaction equation would predict to be the perceived motion-in-depth and deformation, and hence the perceived speed, of our random dot stimuli as a function of the free parameter, λ. The cost function, H, is minimised by setting:

$$\frac{\partial H}{\partial \alpha_p} = 0. \quad (2)$$

Details of the solution to Eq. (2) are given in Appendix B.

Fig. 7(a) shows plots of the predicted perceived speed as a function of the λ parameter for the five types of optic flow stimuli from the experiments at the faster base speed (21.3 deg s^{-1} mean speed). For all values of λ less than 0.96, the elaborated **motion-in-depth** hypothesis based on the constraint satisfaction equation predicts that expanding motions will be perceived as faster than corresponding contracting motions, and radial motions as faster than spirals, with rotations perceived as slowest of all. To assess whether the model provides a good fit to the subject data, we found the best fit λ value for each data point in Experiment 1. While we might expect the relative weighting attached to constraints of object rigidity and motion-in-depth to vary from subject to subject, we would want the best-fit λ values for a given subject to remain the same across optic flow types and base speeds.

The best-fit λ values for the data in Experiment 1 are given in Table 1. All the fitted values for λ lie in the range 0.90 ± 0.03, with the exception of CC's expand-

Table 1
Best-fitting values of the model parameter λ (as defined in Eq. (1)) for the subject data from Experiments 1[a]

	CC		SB		CL
	21.3 deg s^{-1}	6.4 deg s^{-1}	21.3 deg s^{-1}	6.4 deg s^{-1}	21.3 deg s^{-1}
Expansion	0.90	0.88	0.93	0.93	0.90
Expanding spiral	0.87	0.85	0.93	0.92	0.88
Contracting spiral	0.90	0.93	0.91	*	0.90
Contraction	0.91	0.93	0.91	0.93	0.91

* Out of range.

[a] Note that the subject SB's perceived speed value for 6.4 deg s^{-1} contracting spirals could not be fitted as it fell out of the range of predictions made by the model.

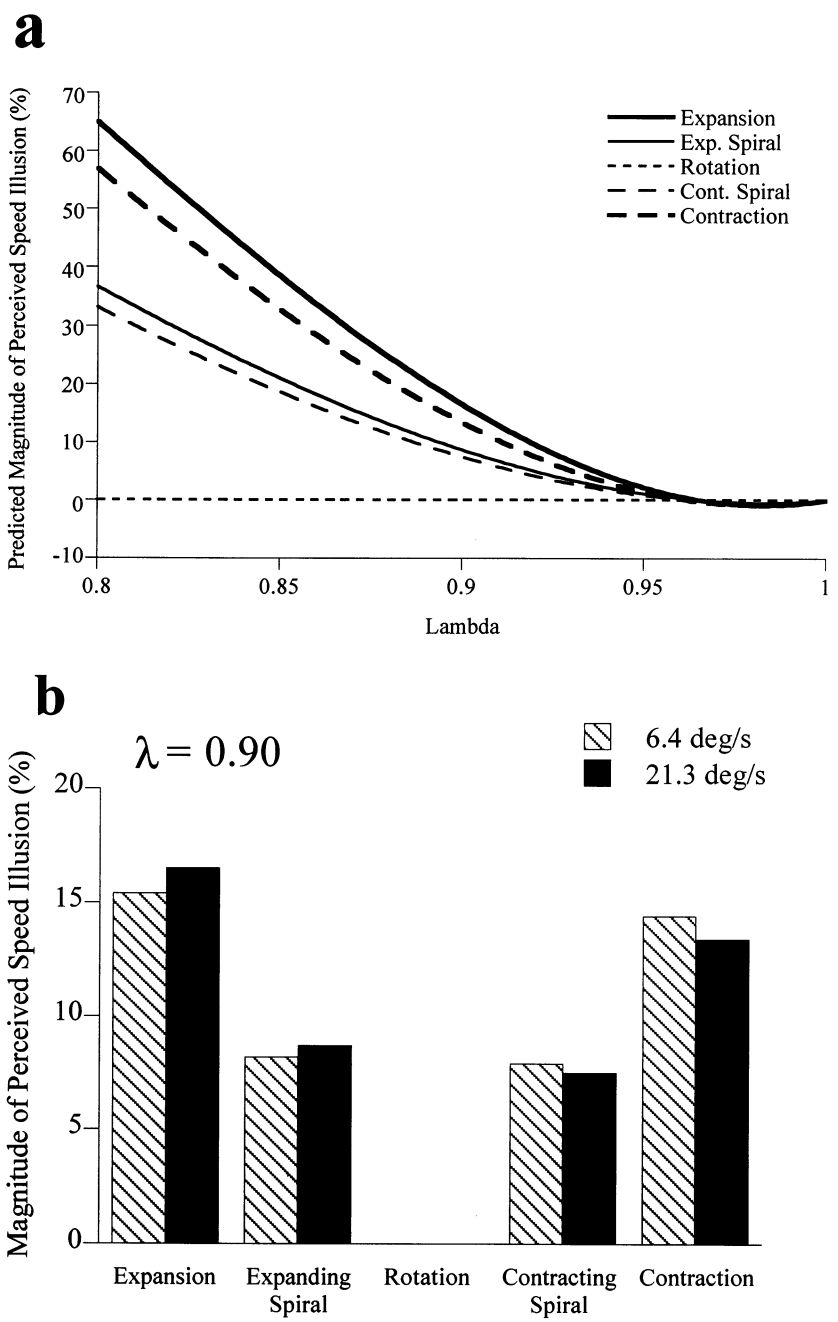

Fig. 7. (**a**) Predictions of a model of speed perception based on the simultaneous satisfaction of constraints on object rigidity and motion-in-depth. The predicted magnitude of the perceived speed illusion for a mean dot speed of 21.3 deg s^{-1} is plotted as a function of the parameter λ defined in Eq. (1). The value of λ determines the relative weighting of the constraints on object rigidity and motion-in-depth, with higher values of λ (up to a maximum of 1) imposing higher penalties on the perception of motion-in-depth. (**b**) The predictions of the model at base speeds of 6.4 and 21.3 deg s^{-1} for a value of $\lambda = 0.90$, for comparison with the subject data of Figs. 1 and 2.

ing spiral data at the slower speed ($\lambda = 0.85$), although it should be noted that it was not possible to fit SB's contracting spiral data as it fell outside the range of model predictions. For the individual subjects, λ values for CC lay in the range 0.89 ± 0.04, 0.92 ± 0.01 for SB, and 0.89 ± 0.02 for CL. For comparison with the subject data of Figs. 1 and 2, the predictions of the model for a value of $\lambda = 0.90$ are shown in Fig. 7(b). The fact that the fitted λ values for the subject data are clustered around 0.9 suggests that, under these experimental conditions at least, constraints primarily on motion-in-depth and to a lesser extent on object rigidity influence the way in which motion with a radial component is interpreted.

6. Conclusion

The results of Experiment 1 show that the perceived speed of complex motion stimuli depends upon the pattern of global motion, while the speed discrimination thresholds measured in Experiment 2 do not depend on the type of complex motion. We find that the perceived speed results are more easily accounted for by a model satisfying simultaneous constraints on motion-in-depth and object rigidity than by the hypothesis that they are a perceptual correlate of a possible bias toward expansions in the tuning of complex motion detectors in the human visual system. Speed discrimination thresholds for complex motions containing a global pattern of direction information and a radial speed gradient were found to be no lower than for stimuli with identical speed profiles but no global pattern of direction information, suggesting that speed discrimination is based on the pooled responses of elementary motion detectors.

Acknowledgements

This work was supported by NIH Grant EY-2ROI-0781-08 to LMV. The stimulus generation programs were based on a suite of psychophysics software written for the Brain & Vision Research Laboratory by Jose Diaz.

Appendix A. Implementation of complex motion stimuli

A.1. Equations of motion

The velocity field in polar co-ordinates (r, θ), of an arbitrary spiral pattern centred on the origin is given by:

$$\begin{pmatrix}\dot{r}\\ \dot{\theta}\end{pmatrix} = \omega\begin{pmatrix}r\cos\varphi\\ \sin\phi\end{pmatrix} \tag{A1}$$

where ϕ is the flow angle of the motion in optical flow space and ω determines the speed of the motion. In the case where $\phi = \pm 90°$, the equation defines a pure rotation with an angular speed of ω. For radial motions (expansion: $\phi = 0°$; contraction: $\phi = 180°$) speed is proportional to distance from the origin.

We implement complex motion using patterns of dots initially positioned randomly within the stimulus aperture. For each dot, we must calculate its position in the following frame. For a dot positioned at a point (r_0, θ_0), the position at time Δt later is obtained as follows from Equation A1:

$$\frac{\mathrm{d}r}{\mathrm{d}t} = r\,\omega\cos\phi \tag{A2}$$

Rearranging and integrating both sides gives:

$$\int_{r_0}^{r_t}\frac{\mathrm{d}r}{r} = \int_0^{\Delta t}\omega\cos\phi\ \mathrm{d}t \tag{A3}$$

which solves to give:

$$r_t = r_0\ \mathrm{e}^{\omega\,\Delta t\cos\phi} \tag{A4}$$

where r_t is the distance of the dot from the origin at time Δt after it was at r_0.

Similarly, for the angular position, θ_t, Eq. (1) gives:

$$\frac{\mathrm{d}\theta}{\mathrm{d}t} = \omega\sin\phi \tag{A5}$$

$$\int_{\theta_0}^{\theta_t}\mathrm{d}\theta = \int_0^{\Delta t}\omega\sin\phi\ \mathrm{d}t \tag{A6}$$

$$\theta_t = \theta_0 + \omega\,\Delta t\sin\phi \tag{A7}$$

Eqs. (A4) and (A7) define the motion of any given dot under a complex motion specified in terms of its flow angle, ϕ, and the speed parameter, ω. To calculate the new position of the dot after one frame of an image sequence, we simply set $\Delta t = 1$. In order to implement the complex motion on a computer monitor we must transform to Cartesian co-ordinates. To simplify the transformation, note that Eq. (A4) defines an enlargement about the origin. In Cartesian co-ordinates, the equation for an enlargement is:

$$\begin{pmatrix}x'\\ y'\end{pmatrix} = \alpha\begin{pmatrix}x\\ y\end{pmatrix} \tag{A8}$$

where α is the scale factor. Rotation by an angle, β, about the origin is given by:

$$\begin{pmatrix}x'\\ y'\end{pmatrix} = \begin{pmatrix}x\cos\beta - y\sin\beta\\ x\sin\beta + y\cos\beta\end{pmatrix} \tag{A9}$$

Thus, for motion between successive frames (i.e. $\Delta t = 1$), Eqs. (A4) and (A8) give us:

$$\alpha = \mathrm{e}^{\omega\cos\phi} \tag{A10}$$

and Eqs. (A7) and (A9) give:

$$\beta = \omega\sin\phi \tag{A11}$$

Combining the transformations in Eqs. (A8) and (A9), and substituting in the expressions for α and β, gives:

$$\begin{pmatrix}x_t\\ y_t\end{pmatrix} = \mathrm{e}^{\omega\cos\phi}\begin{pmatrix}x_0\cos(\omega\sin\phi) - y_0\sin(\omega\sin\phi)\\ x_0\sin(\omega\sin\phi) + y_0\cos(\omega\sin\phi)\end{pmatrix} \tag{A12}$$

This expression determines the position of each dot after each frame of the image sequence.

A.2. Wraparound and maintaining constant dot density

In our computer implementation, the position of each dot after each frame is determined by the following steps:

(1) **Motion**: calculate the position of the dot after motion.

(2) **Wraparound**: check if dot is still inside stimulus aperture. If not, reposition according to wraparound procedure.

A.3. Wraparound procedure:

The stimulus aperture we use is an annulus with an outer radius of 12° and an inner radius of 2°. During expansion all dots move away from the focus of expansion. This will cause some dots to fall outside of the stimulus aperture. Conversely, during contraction some dots will fall inside the inner ring of the annulus. In order to maintain a constant density of dots within the stimulus aperture, these dots must be repositioned inside the annulus. We term this repositioning process 'wraparound'. It is important to maintain a constant density of dots across the stimulus in order to avoid artifactual cues of stimulus density which might influence the psychophysical decisions subjects are required to make. Here we describe the procedure used to wrap dots which fall outside the stimulus during expansion. To generate contracting stimuli, we use an identical procedure and then run the image sequence backwards.

In the first frame of the stimulus, the dots are positioned randomly within the stimulus aperture so that the expected density of dots per unit area is uniform across the stimulus. Fig. 8 schematically shows the expected distribution of dots within the stimulus as a function of distance from the centre of the aperture.

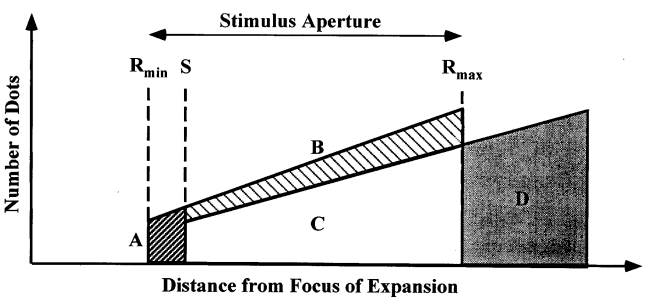

Fig. 8. Schematic diagram of the distribution of dots in the stimulus as a function of distance from the centre of motion. Initially, dots are distributed uniformly over area, hence linearly with radius between the inner and outer apertures of the stimulus ($R_{\min}$ and $R_{\max}$). The initial dot distribution corresponds to the union of regions A, B and C. One frame of motion with an expanding component corresponds to a rescaling of the abscissa. The effects of rescaling are 3-fold: (1) region A near the inner aperture is evacuated of dots; (2) the dot density of the remainder of the stimulus decreases by a certain factor; (3) some dots are repositioned outside the outer aperture (region D). To maintain constant dot density, dots falling outside the stimulus aperture (i.e. in region D) must be repositioned in regions A and B. Details of the 'wraparound' procedure for repositioning dots are given in the text of Appendix A. Note that to generate stimuli with a contracting component, the above procedure was employed and the kinematograms then run backwards.

For the first frame of the stimulus, the number of dots is given by the total area of regions A, B and C. We see that the number of dots increases linearly with distance from the centre (since the area of an annulus of width dr is $2\pi r\ dr$) for all values within the stimulus aperture.

The expansive component of motion corresponds to a rescaling of the abscissa in the diagram, which can be visualised as stretching the expected dot distribution in all directions away from the centre of the stimulus. Hence, after one frame of motion, the expected distribution of dots is given by the union of regions C and D. However, region D lies outside the stimulus aperture. In order to maintain the initial dot distribution, it is necessary to reposition the dots in region D to replace those which have left regions A and B.

First we must calculate the relative areas of regions A and B, so that we determine the probability that a dot from region D should be repositioned in one as opposed to the other. Let the slope of the initial dot distribution be m_0, and that after motion be m_1. Then the area of region A is given by:

$$\text{area(A)} = \int_{R_{\min}}^{S} m_0\, r\ dr = \frac{m_0}{2}(S^2 - R_{\min}^2) \tag{A13}$$

and that of region B by:

$$\text{area(B)} = \int_{S}^{R_{\max S}} (m_0 - m_1)\, r\ dr = \frac{(m_0 - m_1)}{2}(R_{\max}^2 - S^2) \tag{A14}$$

If the dot distribution is rescaled between frames by a factor α, then:

$$m_0 = m_1\ \alpha \tag{A15}$$

and

$$S = \alpha\ R_{\min} \tag{A16}$$

A dot from region D should be repositioned in region A with probability, $p(\text{A})$, given by:

$$p(A) = \frac{\text{area(A)}}{\text{area(A)} + \text{area(B)}} \tag{A17}$$

which solves to:

$$p(\text{A}) = \frac{\alpha\ (1+\alpha) R_{\min}^2}{\alpha\ R_{\min}^2 + R_{\max}^2} \tag{A18}$$

and in region B with probability $p(\text{B}) = 1 - p(\text{A})$.

Once we have determined in which region a dot is to be repositioned, we then have to calculate its new location within that region. This is achieved by choosing a position at random from the relevant region. However, the required distribution of dots is not uniform with respect to distance from the centre of the aperture, so we must transform the pseudorandom number we obtain from the computer's random number generator according to the fundamental transformation law of probabilities (Press, Flannery, Teukolsky & Vet-

terling, 1988). For region A, the new position of the dot, (R_A, θ_A), is given by:

$$R_A = R_{min}\sqrt{(\alpha^2 - 1)\, X + 1} \tag{A19}$$

where X is a random deviate uniform over the range 0 to 1, and for region B:

$$R_B = \sqrt{(R_{max}^2 - \alpha^2 R_{min}^2)\, X + \alpha^2 R_{min}^2} \tag{A20}$$

The angular position, θ_A or θ_B, of wrapped-around dots is selected randomly from a uniform distribution (0, 360).

Appendix B. Modelling the perceived speed of complex motions

B.1. Calculating the mean speed of complex motion stimuli

Let there be N dots each moving with velocity $\mathbf{v}_i$ in a complex motion stimulus. The speed of each dot, v_i, is simply the magnitude of $\mathbf{v}_i$, $|\mathbf{v}_i|$. The mean speed of dot motion in the stimulus is given by:

$$\bar{v} = \frac{\sum_i^N |\mathbf{v}_i|}{N} \tag{B1}$$

Let r denote distance from the centre of motion of the stimulus. If the dot positions are drawn from a probability distribution uniform over angle, $f(r)$, and dot speed is a function only of radius, then the expected value of the mean dot speed is:

$$\langle \bar{v} \rangle = \frac{\int_{R_{min}}^{R_{max}} f(r)\, v(r) \mathrm{d}r}{\int_{R_{min}}^{R_{max}} f(r) \mathrm{d}r} \tag{B2}$$

In order for the expected dot density to be uniform over area, $f(r)$ must increase linearly with radius ($f(r) \propto r$). For optic flow stimuli, dot speed is also proportional to radius ($v(r) = \omega\ r$) where ω is the angular speed of the stimulus. For $f(r) \propto r$, $v(r) = \omega\ r$, Eq. (B2) solves to:

$$\langle \bar{v} \rangle = \frac{2\omega}{3}\left(\frac{R_{max}^3 - R_{min}^3}{R_{max}^2 - R_{min}^2}\right) \tag{B3}$$

B.2. Perceived speed and motion-in-depth

Let us now consider the case where a complex motion stimulus is seen to move both in the plane of the stimulus and in depth relative to the observer. Let the distance of the screen from the observer be z, and the perceived speed of motion in the plane be $u_p(r) = \omega' r$. If the plane of the stimulus is perpendicular to the line of sight of the observer, then the speed of a dot is consistent with its motion in the plane and in depth, $v_p(r)$, is given by:

$$v_p(r) = \sqrt{\omega'^2 r^2 + \dot{z}^2} \tag{B4}$$

where the dot denotes differentiation with respect to time.

Replacing $v(r)$ with $v_p(r)$ in Eq. (B2), and substituting in the expression for $v_p(r)$ given in Eq. (B4) allows us to obtain an expression for the expected mean perceived speed of the dot stimulus for a given perceived angular speed of motion-in-the-plane, ω', and perceived motion-in-depth. The resulting expression is:

$$\langle \bar{v}_p \rangle = \frac{2\omega'}{3}\left(\frac{\left(R_{max}^2 + \left(\frac{\dot{z}}{\omega'}\right)^2\right)^{\frac{3}{2}} - \left(R_{min}^2 + \left(\frac{\dot{z}}{\omega'}\right)^2\right)^{\frac{3}{2}}}{R_{max}^2 - R_{min}^2}\right) \tag{B5}$$

B.3. Satisfying joint constraints on object rigidity and motion-in-depth

To obtain predictions of perceived speed using Eq. (B5), we first need values for the perceived angular speed of motion-in-the-plane and the perceived motion-in-depth. We already have one expression (Eq. (1)) linking perceived motion-in-depth (Δz) with perceived motion-in-the-plane (α_p) through a joint constraint satisfaction. We can also relate Δz and α_p through the geometry of image formation, allowing us to solve for the values of both. The geometrical constraint we use, which we term the line-of-sight constraint, is that the perceived position in 3-D space of any given dot in the random dot pattern must lie along the line of sight from the observer to the dot's actual position (see Fig. 6).

Let α be the scale factor of the enlargement of the dot pattern between frames (see Eq. (A8)) and β the angle of rotation about the origin (see Eq. (A9)). Then the transformation matrix, $\mathbf{M}$, describing the actual motion of the dots in 3-D space is given by:

$$\mathbf{M} = \begin{pmatrix} \alpha\cos\beta & -\alpha\sin\beta & 0 \\ \alpha\sin\beta & \alpha\cos\beta & 0 \\ 0 & 0 & 1 \end{pmatrix}. \tag{B6}$$

We can define the perceived motion-in-the-plane similarly as:

$$\mathbf{M}_P = \begin{pmatrix} \alpha_p\cos\beta_p & -\alpha_p\sin\beta_p & 0 \\ \alpha_p\sin\beta_p & \alpha_p\cos\beta_p & 0 \\ 0 & 0 & 1 \end{pmatrix}, \tag{B7}$$

where α_p and β_p are the perceived enlargement and rotation within the plane, respectively. Since the rotational motion of the dot pattern cannot be interpreted as motion-in-depth, we assume it is perceived veridi-

cally (i.e. $\beta_p = \beta$). If we define the perceived motion-in-depth, $\mathbf{T}_p$, as:

$$\mathbf{T}_p = \begin{pmatrix} 0 \\ 0 \\ -\Delta z \end{pmatrix} \tag{B8}$$

then we can express the **line-of-sight** constraint in the following equation:

$$\mathbf{x}' = k(\mathbf{M}\mathbf{x}) = \mathbf{M}_P\mathbf{x} + \mathbf{T}_P, \tag{B9}$$

where $\mathbf{x}$ is the actual position of any given dot relative to the observer at time $t - \Delta t$, $\mathbf{M}\mathbf{x}$ is the actual position at time t, $\mathbf{x}'$ is the perceived position at time t, and k is a scalar.

Substituting Eqs. (B6), (B7) and (B8) into Eq. (B9) and simplifying gives an expression for motion-in-depth, Δz, in terms of absolute depth, z, and actual and perceived radial motion within the plane, α and α_p:

$$\Delta z = \left(\frac{\alpha - \alpha_p}{\alpha}\right) z\,. \tag{B10}$$

The expression for Δz in Eq. (B10) can now be substituted into Eq. (1), the expression for the cost function, H, in terms of Δz and α_p. Minimising H by differentiating partially with respect to α_p gives us an expression for the perceived radial motion, α_p, in terms of the actual radial motion, α, and λ, the parameter determining the relative weighting of the two constraints:

$$\alpha_p = \alpha\left(\frac{\lambda + \alpha(1-\lambda)}{\lambda + \alpha^2(1-\lambda)}\right). \tag{B11}$$

Finally, to obtain our predictions for perceived speed we must express the unknowns in Eq. (B5) in terms of α_p and Δz. The rate of change of depth with time is given by the discrete approximation:

$$\dot{z} = \frac{\Delta z}{\Delta t}\,, \tag{B12}$$

where Δt is the duration of a single frame. The perceived angular speed of motion-in-the-plane, ω', can be obtained from the perceived rates of radial and rotational motion, ω'_{rad} and ω'_{rot}, as simply:

$$\omega' = \sqrt{\omega'^2_{rad} + \omega'^2_{rot}}\,. \tag{B13}$$

Assuming that the rotational component of motion is perceived veridically, as it has no possible interpretation as motion-in-depth:

$$\omega'_{rot} = \omega_{rot} = \omega \sin\phi\,, \tag{B14}$$

where ϕ is the flow angle of the complex motion stimulus and ω is its actual angular speed, as defined in Eq. (A1). We can thus write ω' as:

$$\omega' = \sqrt{q^2\,\omega^2\cos^2\phi + \omega^2\sin^2\phi}\,, \tag{B15}$$

where q is given by the logarithm of the ratio of the perceived and actual rates of expansion, α_p and α (see Eq. (A10)):

$$q = \ln\left(\frac{\alpha_p}{\alpha}\right). \tag{B16}$$

The values of the perceived rate of change of depth with time and perceived speed of angular motion-in-the-plane obtained from Eqs. (B12) and (B15) can then be substituted into Eq. (B5) to give a value for perceived speed. Alternatively, rather than calculate the perceived speed explicitly, we can calculate the ratio of the perceived speed of a given optic flow pattern relative to a rotation by computing the ratio of the expressions in Eqs. (B3) and (B5):

$$\Psi = \frac{\omega'}{\omega}\left(\frac{\left(R^2_{max} + \left(\frac{\dot{z}}{\omega'}\right)^2\right)^{\frac{3}{2}} - \left(R^2_{min} + \left(\frac{\dot{z}}{\omega'}\right)^2\right)^{\frac{3}{2}}}{R^3_{max} - R^3_{min}}\right) \tag{B17}$$

where Ψ is the perceived speed ratio plotted as a function of λ in Fig. 7(a) for a range of optic flows.

References

Albright, T. D., & Desimone, R. (1987). Local precision of visuotopic organization in the middle temporal area (MT) of the macaque. *Experimental Brain Research*, *65*, 582–592.

Bex, P. J., & Makous, W. (1997). Radial motion looks faster. *Vision Research*, *37*, 3399–3405.

Bex, P. J., Metha, A. B., & Makous, W. (1998). Psychophysical evidence for a functional hierarchy of motion processing mechanisms. *Vision Research*, *38*, 769–776.

De Bruyn, B., & Orban, G. A. (1988). Human velocity and direction discrimination measured with random dot patterns. *Vision Research*, *28*, 1323–1335.

De Bruyn, B., & Orban, G. A. (1990). The importance of velocity gradients in the perception of three-dimensional rigidity. *Perception*, *19*, 21–27.

Duffy, C. J., & Wurtz, R. H. (1991). Sensitivity of MST neurons to optic flow stimuli. I.A continuum of response selectivity to large-field stimuli. *Journal of Neurophysiology*, *65*, 1329–1345.

Duffy, C. J., & Wurtz, R. H. (1991). Sensitivity of MST neurons to optic flow stimuli. II. Mechanisms of response selectivity revealed by small-field stimuli. *Journal of Neurophysiology*, *65*, 1346–1359.

Duffy, C. J., & Wurtz, R. H. (1997). Planar directional contributions to optic flow responses in MST neurons. *Journal of Neuroscience*, *17*, 2839–2851.

Freeman, T. C. A., & Harris, M. G. (1992). Human sensitivity to expanding and rotating motion: effects of complementary masking and directional structure. *Vision Research*, *32*, 81–87.

Geesaman, B. J., & Andersen, R. A. (1996). The analysis of complex motion patterns by form/cue invariant MSYd neurons. *Journal of Neuroscience*, *16*, 4716–4732.

Geesaman, B. J., Born, R. T., Andersen, R. A., & Tootell, R. B. H. (1997). Maps of complex motion selectivity in the superior temporal cortex of the alert macaque monkey: a double-label 2-deoxyglucose study. *Cerebral Cortex*, *7*, 749–757.

Geesaman, B. J., & Qian, N. (1996). A novel speed illusion involving expansion and rotation patterns. *Vision Research*, *36*, 3281–3292.

Geesaman, B. J., & Qian, N. (1998). The effect of complex motion pattern on speed perception. *Vision Research*, *38*, 1223–1231.

Graziano, M. S. A., Anderson, R. A., & Snowden, R. J. (1994). Tuning of MST neurons to spiral motions. *Journal of Neuroscience*, *14*, 54–67.

Harris, M. G., Freeman, T. C. A., & Tyler, P. A. (1994). Human sensitivity to temporal proximity: the role of spatial and temporal speed gradients. *Perception & Psychophysics*, *55*, 689–699.

Kim, J.-N., Mulligan, K., & Sherk, H. (1997). Simulated optic flow and extrastriate cortex. I. Optic flow versus texture. *Journal of Neurophysiology*, *77*, 554–561.

Krapp, H. G., & Hengstenberg, R. (1996). Estimation of self-motion by optic flow processing in single visual interneurons. *Nature*, *384*, 463–466.

Lagae, L., Maes, H., Raiguel, S., Xiao, D.-K., & Orban, G. A. (1994). Responses of macaque STS neurons to optic flow components: a comparison of areas MT and MST. *Journal of Neurophysiology*, *71*, 1597–1626.

Lee, D. N. (1980). The optic flow field: the foundation of vision. *Philosophical Transactions of the Royal Society of London B*, *290*, 169–179.

McKee, S. P. (1981). A local mechanism for differential velocity detection. *Vision Research*, *21*, 491–500.

Morrone, M. C., Burr, D. C., & Vaina, L. M. (1995). Two stages of visual processing for radial and circular motion. *Nature*, *376*, 507–509.

Mulligan, K., Kim, J.-N., & Sherk, H. (1997). Simulated optic flow and extrastriate cortex. II. Responses to bar versus large-field stimuli. *Journal of Neurophysiology*, *77*, 562–570.

Orban, G. A., Lagae, L., Verri, A., Raiguel, S., Xiao, D.-K., Maes, H., & Torre, V. (1992). First-order analysis of optical flow in monkey brain. *Proceedings of the National Academy of Sciences USA*, *89*, 2595–2599.

Press, W. H., Flannery, B. P., Teukolsky, S. A., & Vetterling, W. T. (1988). *Numerical recipes in C*. Cambridge: Cambridge University Press.

Regan, D., & Beverley, K. I. (1985). Visual responses to vorticity and the neural analysis of optic flow. *Journal of the Optical Society of America*, *A2*, 280–283.

Saito, H. A., Yukie, M., Tanaka, K., Hikosaka, K., Fukada, Y., & Iwai, E. (1986). Integration of direction signals of image motion in the superior temporal sulcus of the macaque monkey. *Journal of Neuroscience*, *6*, 145–157.

Sekuler, A. B. (1992). Simple-pooling of unidirectional motion predicts speed discrimination for looming stimuli. *Vision Research*, *32*, 2277–2288.

Smith, A. T., Snowden, R. J., & Milne, A. B. (1994). Is global motion really based on spatial integration of local motion signals? *Vision Research*, *34*, 2425–2430.

Snowden, R. J. (1994). Motion processing in the primate cerebral cortex. In A. T. Smith, & R. J. Snowden, *Visual detection of motion*. London: Academic Press Ltd.

Snowden, R. J., & Milne, A. B. (1996). The effects of adapting to complex motions: position invariance and tuning to spiral motions. *Journal of Cognitive Neuroscience*, *8*, 412–429.

Snowden, R. J., & Milne, A. B. (1997). Phantom motion aftereffects—evidence of detectors for the analysis of optic flow. *Current Biology*, *7*, 717–722.

Tanaka, K., Fukada, Y., & Saito, H. (1989). Underlying mechanisms of the response selectivity of expansion/contraction and rotation cells in the dorsal part of the medial superior temporal area of the macaque monkey. *Journal of Neurophysiology*, *62*, 642–656.

Tanaka, K., Hikosaka, K., Saito, H., Yukie, M., Fukada, Y., & Iwai, E. (1986). Analysis of local and wide-field movements in the superior temporal visual areas of the macaque monkey. *Journal of Neuroscience*, *6*, 134–144.

Tanaka, K., & Saito, H. (1989). Analysis of motion of the visual field by direction, expansion/contraction, and rotation cells clustered in the dorsal part of the medial superior temporal area of the macaque monkey. *Journal of Neurophysiology*, *62*, 626–641.

van der Grind, W. A., van Doorn, A. J., & Koenderink, J. J. (1983). Detection of coherent movement in peripherally viewed random-dot patterns. *Journal of the Optical Society of America A*, *73*, 1674–1683.

Verghese, P., & Stone, L. S. (1995). Combining speed information across space. *Vision Research*, *35*, 2811–2823.

Verghese, P., & Stone, L. S. (1996). Perceived visual speed constrained by image segmentation. *Nature*, *381*, 161–163.

Watamaniuk, S. N. J., & Sekuler, R. (1992). Temporal and spatial integration in dynamic random-dot stimuli. *Vision Research*, *32*, 2341–2347.

Wylie, D. R. W., Bischof, W. F., & Frost, B. J. (1998). Common reference frame for neural coding of translational and rotational optic flow. *Nature*, *392*, 278–282.

Zemel, R. S., & Sejnowski, T. J. (1998). A model for encoding multiple object motions and self-motion in area MST of primate visual cortex. *Journal of Neuroscience*, *18*, 531–547.